Acta Mechanica Sinica (2014) 30(5):746–761
DOI 10.1007/s10409-014-0063-4

RESEARCH PAPER

Coupled lateral-torsional-axial vibrations of a helical gear-rotor-bearing system

Chao-Feng Li · Shi-Hua Zhou · Jie Liu · Bang-Chun Wen

Received: 12 October 2013 / Revised: 27 February 2014 / Accepted: 1 April 2014

Abstract Considering the axial and radial loads, a mathematical model of angular contact ball bearing is deduced with Hertz contact theory. With the coupling effects of lateral, torsional and axial vibrations taken into account, a lumped-parameter nonlinear dynamic model of helical gear-rotor-bearing system (HGRBS) is established to obtain the transmission system dynamic response to the changes of different parameters. The vibration differential equations of the drive system are derived through the Lagrange equation, which considers the kinetic and potential energies, the dissipative function and the internal/external excitation. Based on the Runge–Kutta numerical method, the dynamics of the HGRBS is investigated, which describes vibration properties of HGRBS more comprehensively. The results show that the vibration amplitudes have obvious fluctuation, and the frequency multiplication and random frequency components become increasingly obvious with changing rotational speed and eccentricity at gear and bearing positions. Axial vibration of the HGRBS also has some fluctuations. The bearing has self-variable stiffness frequency, which should be avoided in engineering design. In addition, the bearing clearance needs little attention due to its slightly discernible effect on vibration response. It is suggested that a careful examination should be made in modelling the nonlinear dynamic behavior of a helical gear-rotor-bearing system.

The project was supported by the National Natural Science Fundation of China (51105063) and the Fundamental Research Funds for the Central Universities (N120403004).

C.-F. Li (✉) · S.-H. Zhou · B.-C. Wen
School of Mechanical Engineering & Automation,
Northeastern University, 110819 Shenyang, China
e-mail: chfli@mail.neu.edu.cn

J. Liu
School of Mechanical Engineering,
Shenyang University of Technology,
110870 Shenyang, China

Keywords Helical gear-rotor-bearing system · Coupled lateral-torsional-axial vibration · Meshing frequency · Nonlinear dynamics

1 Introduction

It is known that the gear rotor bearing system plays an important role in many sorts of machinery. A failure of the drive system may cause breakdown of the whole machinery and major economic loss. In the gear transmission system, helical gear could produce radial, tangential and axial forces on the mesh point, which can cause lateral vibration, torsional vibration, axial vibration and even the coupled lateral-torsional-axial vibration. The dynamic characteristics and performances have important influence on the entire machine [1–3]. In rotational industry, the study on vibration characteristics of individual component, such as gear pair, shaft, gear, and bearing, has been established as an important part of the design. However, the vibration characteristic of an individual component can change considerably when these components are assembled together to form one system due to the coupled effects among these constituent components. Due to the helical gear meshing of a gear pair, the gear-rotor-bearing system (HGRBS) has different vibration characteristics as compared with a simplified rotor system. One of the main features of HGRBS model is that it has coupled lateral-torsional-axial vibration between the driving shaft and the driven shaft. If not taken into consideration, the effect of coupled vibration can not only reduce the calculation accuracy, but also lose some important characteristics of the HGRBS (torsional excitation excites the lateral response, coupled vibration causes new frequency component). Therefore, it is important to establish an accurate model for dynamic characteristics of the HGRBS. In recent years, many scholars did a lot of researches and experiments to analyze the dynamic characteristics of helical gear-rotor-bearing systems, and reached some remarkable achievements. A number of models were proposed to describe the dynamic behavior of helical gear systems [4–21]. On the basis of gear dynamic model, Kaharman et al. [4, 5] studied the nonlinear characteristics of gear systems with harmonic balance and Runge–Kutta methods, and solved the nonlinear dynamic response of spur gear systems. In order to consider the effect of time-varying mesh stiffness, Al-shyyab and Kaharman et al. [6] sequentially analyzed the influence of the rotor-bearing system with the gear clearance and the time-varying meshing stiffness, and carried out a detailed analysis of the system. Lin et al. [7] and Rao et al. [8] established a torsional vibration model of gear rotor systems, and studied the meshing force, dynamic load factor and tip relief parameter. A dynamic model of the coupled HGRBS was established, in which the lateral-torsional-axial-pendulum motion was considered and the kinetic equation was obtained. It provided effective method for dynamic design of the helical gear system [9, 10]. A model which considered the coupled lateral and torsional nonlinear vibration of the gear meshing and torsional action was established in Refs. [11–13] for a high-speed gear-rotor-bearing system. The dynamic differential equations were deduced for the imbalance rotors. The lateral and torsional vibration response was investigated using numerical simulations. The effects of eccentricity and gear stiffness etc. were studied on the system vibration response. Using finite element and Lagrange methods, the gyroscopic effect and oil film supported were taken into account, and a lateral and torsional vibration model was established to analyze the gear vibration [14]. Wang et al. [15] and Lee et al. [16] established a dynamical model of coupled lateral-tensional-axial-swing motion of two-stage helical gear transmission system, in which time-varying meshing stiffness, meshing error and backlash were taken into consideration. The dynamic equation of the helical gear transmission was solved and dynamic response was calculated. Chen et al. [17] established a dynamic lumped-parameter gear model incorporating the effects of time-varying and asymmetric mesh stiffness and a backlash nonlinearity to analyze the spur gear rattle response under the idling condition. Wu et al. [18] studied the effects of tooth crack on the vibration response of a one-stage gearbox with spur gears. The growth in a tooth crack was reflected in the total mesh stiffness of the gear system. A lumped-parameter model was used to simulate the vibration response of the pair of meshing gears. Walha et al. [19] adopted a gear impact theory based on the work and used lumped stiffness and damping representations to model the supporting bearings. Russo et al. [20] performed a lot of experiments to quantify the effect of lubrication on the idle gear rattle response of helical pairs inside an automotive gearbox. Han et al. [21] developed a new multi-body dynamic model to predict the mesh force during gear rattle. The results show good agreement with the predictions of a single-degree-of-freedom theoretical model that accounts for the oil squeeze effect between the gear teeth during the non-contact phases.

It can be seen from the previous references that most of existing helical gear drive systems were usually regarded as spur gear drive systems, and the axial vibration was ignored. Now HGBRS comprehensively contains actual gear rotational speed, eccentricity, bearing nonlinearity and other factors, and thus using a nonlinear dynamic model to describe the coupled lateral, torsional and axial vibrations is in urgent need. In order to obtain precise analysis and master dynamic characteristics of transmission system, it is necessary to establish precise dynamic model of the HGBRS. A requirement for reliable HGBRS design calculations is sufficient insight in the dynamics of the entire wind turbine drive train.

For accurate analytical modeling which can indicate the meshing relations and the detailed nonlinear characteristics, it needs to establish a mechanics model and suitable mechanism relation model. Few references can be found on the effects of rotational speed, eccentricity and bearing clearance on gear-rotor-bearing systems. In this paper, considering the complex nonlinear characteristic, an analytical model is proposed via lumped-parameter method, which can systematically describe the vibration characteristics of HGRBS. And the model is used to investigate complex, nonlinear dynamic behavior of the HGRBS, in particular the influence of different parameters on vibration characteristics.

2 The lumped-parameter model of HGRBS

Considering the influences of input/output and support bearing et al., the static model of HGRBS is shown in Fig. 1, and the dynamic model of the transmission system is shown in Fig. 2. m_i $(i = 1, 2)$ is the equivalent mass of helical gear. J_i $(i = 1, 2)$ represents rotational inertia. m_{bi} $(i = 1, 2, 3, 4)$ is equivalent mass at bearing position. J_d and J_1 indicate rotational inertia in input/output terminal. ρ_i $(i = 1, 2)$ represents the eccentricity. F_{xi}, F_{yi}, and F_{zi} $(i = 1, 2, 3, 4)$ are nonlinear bearing forces in the x, y, and z directions.

2.1 The lumped-parameter model of HGRBS

In Fig. 1, a fixed coordinate system $A_i - x_i y_i z_i$ $(i = 1, 2)$ is set up at A_i, which is the ideal center of the helical gear. B_i $(i = 1, 2, 3, 4)$ represents the ideal centers of bearings. $O_1(x_1, y_1, z_1)$ and $O_2(x_2, y_2, z_2)$ are the rotation centers of the driving and driven gears; $G_1(x_{g1}, y_{g1}, z_{g1})$ and $G_2(x_{g2}, y_{g2}, z_{g2})$ represent the centroids, respectively. To obtain differential equations of the HGRBS, the stress of the cylindrical gear with helical teeth should be analyzed first. Therefore, the dynamic model of a gear meshing is shown in Fig. 2.

In Fig. 2, ϕ_1 and θ_1 $(j = 1, 2, \mathrm{d}, \mathrm{l})$ are the rotational angle and angular vibration displacement of driving gear, driven gear, input terminal and output terminal. r_{b1} and r_{b2} are the base radiuses of driving and driven gears, respectively. F_t, F_r, and F_a represent the tangential force; radial force and axial force. α_t and α_n are the pressure angles of the pitch circle in the end face and the normal direction. β and β_t are helix angles of the pitch circle and the base circle. α_1 indicates the installation angle between center line and vertical direction.

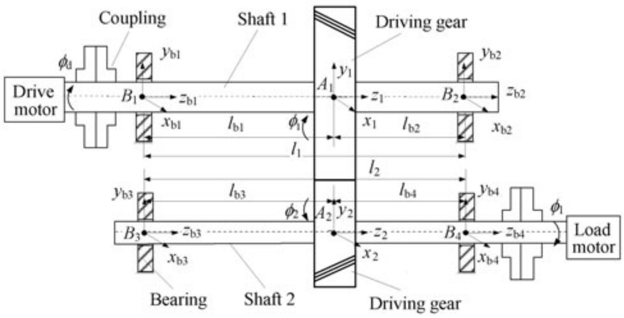

Fig. 1 Static model of a helical gear-shaft-bearing system

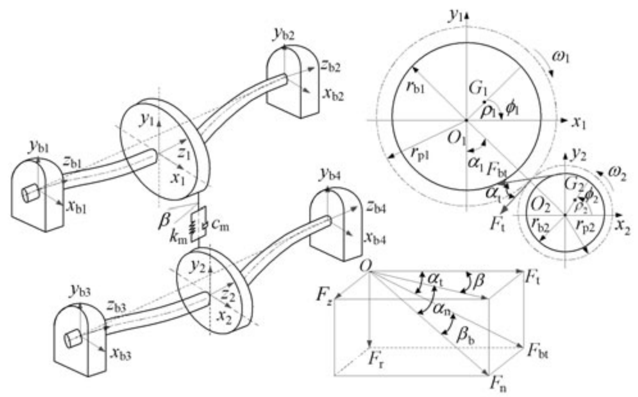

Fig. 2 Dynamic model of a helical gear-rotor-bearing system

According to the geometrical relationships shown in Figs. 1 and 2, the angle displacements of the input/output, driving and driven gears can be expressed by the following equations

$$\begin{aligned} &\phi_d = \omega_1 t + \theta_d, \quad \phi_1 = \omega_1 t + \theta_1, \\ &\phi_2 = \omega_2 t + \theta_2, \quad \phi_1 = \omega_2 t + \theta_1. \end{aligned} \tag{1}$$

The relationships between $G_1(x_{gl}, y_{gl}, z_{gl})$, $G_2(x_{g2}, y_{g2}, z_{g2})$ and $O_1(x_1, y_1, z_1)$, $O_2(x_2, y_2, z_2)$ are expressed as follows

$$\begin{aligned} &x_{gl} = x_1 + \rho_1 \cos(-\phi_1), \quad && x_{g2} = x_2 + \rho_2 \cos\phi_2, \\ &y_{gl} = y_1 + \rho_1 \sin\phi_1, && y_{g2} = y_2 + \rho_2 \sin(-\phi_2), \\ &z_{gl} = z_1, && z_{g2} = z_2. \end{aligned} \tag{2}$$

In order to ensure the contact of teeth surface on meshing performance, it is assumed that the relative deformation of gear pair is completely changed into elastic deformation on teeth surface along the mesh line direction. The meshing gear pair is connected through spring and damping. Therefore, the comprehensive deformation between the driving and the driven gear along the mesh line direction is expressed as

$$\begin{aligned} \delta = {} & (r_{b1}\theta_1 - r_{b2}\theta_2) + [(x_1 + \rho_1 \cos\phi_1) - (x_2 + \rho_2 \cos\phi_2)] \\ & \times \cos(\alpha_1 - \alpha_t) + [(y_1 - \rho_1 \sin\phi_1) - (y_2 + \rho_2 \sin\phi_2)] \\ & \times \sin(\alpha_1 - \alpha_t) + (z_1 - z_2)\tan\beta - e(t). \end{aligned} \tag{3}$$

Calculate and simulate the gear meshing force based on the viscoelasticity theory. The meshing force can be described as

$$F = c_m \dot{\delta} + k_m \delta, \tag{4}$$

where k_m and c_m represent the average meshing stiffness and damping; r_{b1} and r_{b2} are the base radii of helical gears; $e(t)$ indicates the general transmission error, which can be described as follows

$$e(t) = e_0 + e_r \sin(\omega_e t + \phi_e), \tag{5}$$

where e_0 and e_r are the mean and the amplitude of meshing error, ϕ_e is initial position angle. $\omega_e = 2\pi n_1 z_1/60$. z_1 indicates the tooth number of driving gear.

It is assumed that the dynamic meshing force is positive when it points from the driving gear to the driven gear. So the meshing forces in the x, y, and z directions can be respectively described as

$$\begin{aligned} &F_x = F\cos(\alpha_1 - \alpha_t), \\ &F_y = F\sin(\alpha_1 - \alpha_t), \\ &F_z = F\tan\beta. \end{aligned} \tag{6}$$

2.2 External excitation

The input torque (T_{in}) of the helical gear-rotor-bearing system (HGRBS) can be expressed by the following equation

$$T_{in} = T_{inm} + T_{inr}\sin(\omega t + \phi). \tag{7}$$

The output torque (T_{out}) of HGRBS can be calculated from the input torque of the system as

$$T_{out} = T_{in}/i, \tag{8}$$

where T_{inm} is the mean of the input torque, T_{in} represents the amplitude of the input torque, ω is the angular velocity of the system, i represents the transmission ratio of the HGRBS.

2.3 Dynamic model of the angular contact ball bearing

Angular contact ball bearing model is shown in Fig. 3. Bearing outer ring is fixed in the bearing chock, and inner ring is fixed in the shaft. The balls are uniformly distributed between outer ring and inner ring. The velocities v_i and v_0 at the contact point between the rolling ball and outer/inner ring can be expressed as

$$v_i = \omega_i r, \quad v_0 = \omega_0 R, \tag{9}$$

where R and r represent the radii of the bearing outer and inner rings, ω_i and ω_0 are the angular velocities.

Assuming that it is pure rolling between ball and outer/inner ring, and the velocity of cage can be expressed as

$$v_b = (v_0 + v_i)/2 = (\omega_0 R + \omega_i r)/2. \tag{10}$$

Generally, the bearing inner ring rotates together with the shaft, and the bearing outer ring is fixed. Utilizing the relationships $\omega_0 = 0$, $\omega_i = \omega$, the angular velocity of the cage is

$$\omega_{\mathrm{b}} = 2v_{\mathrm{b}}/(R + r) = \omega_i r/(R + r). \tag{11}$$

The rotational angle ϕ_i of the i-th rolling ball at t moment can be expressed as

$$\phi_i = \omega_{\mathrm{b}} t + 2\pi(i - 1)/N_{\mathrm{b}}, \quad i = 1, 2, 3, \cdots, N_{\mathrm{b}}, \tag{12}$$

where N_{b} represents the number of rolling ball.

In Fig. 3, d_{b} is the diameter of rolling ball; d indicates the diameter of shaft; d_{i} and d_{o} represent the diameters of the bearing inner and outer orbits, respectively; d_{m} is the diameter of pitch circle, and $d_{\mathrm{m}} = (d_{\mathrm{i}} + d_{\mathrm{o}})/2$.

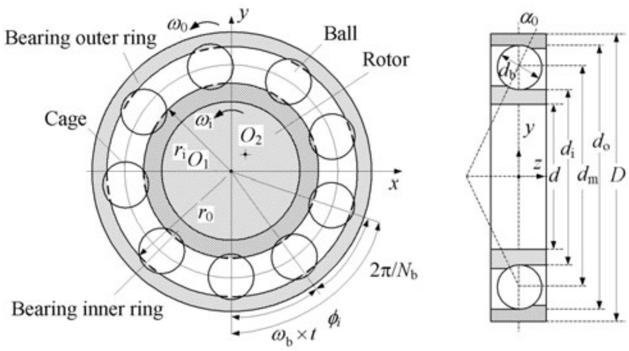

Fig. 3 Schematic diagram of angular contact rolling bearing

When the angular contact ball bearing has a low speed, the centrifugal force and gyroscopic moment can be neglected. F_{r} and F_{a} represent the radial and the axial forces of the bearing, respectively. The ball bearing and the geometric deformation at certain position are shown in Fig. 4.

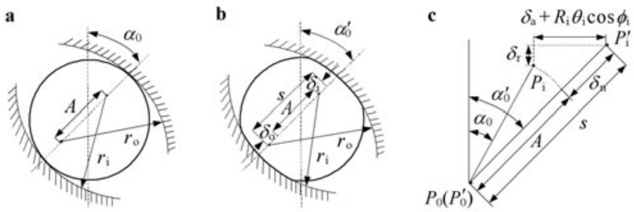

Fig. 4 Ball bearing and geometric deformation at different positions. **a** Before being loaded; **b** After being loaded; **c** Geometric deformation relation

In Fig. 4, α_0 is the initial contacting angle before being loaded, α'_0 indicates the angle after being loaded; P_0 represents the center of the bearing outer ring before being loaded; P'_0 is the center after being loaded. Because the outer ring is fixed, P_0 and P'_0 are the same position; P_{i} is the center of the inner ring before being loaded; P'_{i} represents the center after being loaded; δ_{ai}, δ_{ri}, and θ_{i} are the axial deformation, radial deformation and angular deformation, respectively; R_{i} is the curvature radius of inner orbit; ϕ_{i} is the position angle; δ_{i}, δ_0, and δ_{b} represent the contacting deformation and total deformation between rolling ball and outer and inner orbits.

Because the centrifugal force and the gyroscopic moment are ignored, the contacting angle between rolling ball and bearing orbit and the contacting force are the same. In Fig. 4b, the deformation of rolling ball at position angle ϕ_{i} can be expressed as

$$\delta_{\mathrm{b}} = \delta_{\mathrm{i}} + \delta_{\mathrm{o}} = S - A. \tag{13}$$

According to geometric relationship in Fig. 4c, the distance S between the curvature center of inner orbit and outer orbit can be expressed by the following equation

$$S = [(A\sin\alpha_0 + z + R_{\mathrm{i}}\theta_{\mathrm{i}}\cos\phi_{\mathrm{i}})^2 + (A\cos\alpha_0 + x\cos\phi_{\mathrm{i}} + y\sin\phi_{\mathrm{i}})^2]^{1/2}. \tag{14}$$

The normal contacting deformation between the i-th rolling ball and the bearing orbit is

$$\delta_{\mathrm{b}} = S - A = [(A\sin\alpha_0 + \delta_{\mathrm{a}} + R_{\mathrm{i}}\theta_{\mathrm{i}}\cos\phi_{\mathrm{i}})^2 + (A\cos\alpha_0 + \delta_r)^2]^{1/2} - A. \tag{15}$$

Utilizing the relationships $\delta_{\mathrm{a}} = z$ and $\delta_{\mathrm{r}} = x\cos\phi_{\mathrm{i}} + y\sin\phi_i$, Eq. (13) can be expressed by

$$\delta_{\mathrm{b}} = S - A = [(A\sin\alpha_0 + z + R_{\mathrm{i}}\theta_{\mathrm{i}}\cos\phi_{\mathrm{i}})^2 + (A\cos\alpha_0 + x\cos\phi_{\mathrm{i}} + y\sin\phi_{\mathrm{i}})^2]^{1/2} - A, \tag{16}$$

where x, y, and z represent the vibration displacements respectively; $R_{\mathrm{i}} = d_{\mathrm{m}}/2 + (r_{\mathrm{i}} - d_{\mathrm{b}}/2)\cos\alpha_0$; A is the initial distance between curvature center of inner orbit and outer orbit, and $A = r_{\mathrm{i}} + r_0 + \gamma_0 - d_{\mathrm{b}}$.

At the position angle ϕ_{i}, the actually contacting angular α'_0 can be expressed as

$$\tan\alpha'_0 = \frac{A\sin\alpha_0 + z + R_{\mathrm{i}}\theta_{\mathrm{i}}\cos\phi_{\mathrm{i}}}{A\cos\alpha_0 + x\cos\phi_{\mathrm{i}} + y\sin\phi_{\mathrm{i}}}. \tag{17}$$

According to nonlinear Hertz contact theory, the contact force between the i-th rolling ball and the bearing orbits is $f_{\mathrm{b}i}$, at the same time, the normal stress can be generated between the rolling ball and the bearing orbits only when the $\delta_{\mathrm{b}i}$ is greater than zero. So the force can be expressed by

$$f_{\mathrm{b}i} = K_{\mathrm{c}}(\delta_{\mathrm{b}i})^{3/2}H(\delta_{\mathrm{b}i}). \tag{18}$$

The normal load can be known by Eq. (18), and the axial and radial forces can be expressed as follows

$$\begin{aligned} f_{\mathrm{r}i} &= f_{\mathrm{b}i}\cos\alpha'_0 = K_{\mathrm{c}}(\delta_{\mathrm{b}i})^{3/2}\cos\alpha'_0, \\ f_{\mathrm{a}i} &= f_{\mathrm{b}i}\sin\alpha'_0 = K_{\mathrm{c}}(\delta_{\mathrm{b}i})^{3/2}\sin\alpha'_0. \end{aligned} \tag{19}$$

So the bearing forces ($F_{\mathrm{b}x}$, $F_{\mathrm{b}y}$, and $F_{\mathrm{b}z}$) in the x, y, and z directions can be expressed by

$$
\begin{aligned}
F_{\mathrm{b}x} &= \sum_{i=1}^{N_\mathrm{b}} f_{\mathrm{r}i} \cos\phi_\mathrm{i} \\
&= \sum_{i=1}^{N_\mathrm{b}} K_\mathrm{c}(\delta_{\mathrm{b}i})^{3/2} \cos\alpha_0' H(\delta_{\mathrm{b}i}) \cos\phi_\mathrm{i}, \\
F_{\mathrm{b}y} &= \sum_{i=1}^{N_\mathrm{b}} f_{\mathrm{r}i} \sin\phi_\mathrm{i} \\
&= \sum_{i=1}^{N_\mathrm{b}} K_\mathrm{c}(\delta_{\mathrm{b}i})^{3/2} \cos\alpha_0' H(\delta_{\mathrm{b}i}) \sin\phi_\mathrm{i}, \\
F_{\mathrm{b}z} &= \sum_{i=1}^{N_\mathrm{b}} f_{\mathrm{a}i} = \sum_{i=1}^{N_\mathrm{b}} K_\mathrm{c}(\delta_{\mathrm{b}i})^{3/2} \sin\alpha_0' H(\delta_{\mathrm{b}i}).
\end{aligned} \tag{20}
$$

2.4 Vibration differential equations of the HGRBS

It is assumed that meshing stiffness of the HGRBS is averaged and neglects the meshing backlash, meshing friction and the change of meshing position. The meshing force F along the pressure line direction acts on the center of tooth width. A displacement vector of a helical gear pair can be defined from the pressure line co-ordinate system, as shown in Fig. 2, so

$$
\begin{aligned}
\boldsymbol{X} = [&\theta_\mathrm{d}\ x_{\mathrm{b}1}\ y_{\mathrm{b}1}\ z_{\mathrm{b}1}\ x_1\ y_1\ z_1\ \theta_1\ x_{\mathrm{b}2}\ y_{\mathrm{b}2}\ z_{\mathrm{b}2} \\
&x_{\mathrm{b}3}\ y_{\mathrm{b}3}\ z_{\mathrm{b}3}\ x_2\ y_2\ z_2\ \theta_2\ x_{\mathrm{b}4}\ y_{\mathrm{b}4}\ z_{\mathrm{b}4}\ \theta_l]^\mathrm{T},
\end{aligned} \tag{21}
$$

where θ_d, θ_1, θ_1, and θ_2 represent the angular vibration displacements of input terminal, output terminal, driving gear and driven gear respectively; x_i, y_i, and z_i ($i = 1, 2$) are the linear vibration displacements of driving and driven gears in the x, y, and z directions; $x_{\mathrm{b}i}$, $y_{\mathrm{b}i}$, and $z_{\mathrm{b}i}$ ($i = 1, 2, 3, 4$) indicate the linear vibration displacements of the bearing in the x, y, and z directions, respectively.

According to the dynamic analysis of the HGRBS, with the mesh torque, input/output torque taken into account, the kinetic energy T, the potential energy U and the dissipation function R are established. Utilizing the Lagrange equation, the differential equations of the train system can be expressed as follows.

The vibration differential equations at the input terminal and on the left bearing of driving shaft

$$
\begin{aligned}
&J_\mathrm{d}\ddot{\theta}_\mathrm{d} + c_{\mathrm{t}1}(\dot{\theta}_\mathrm{d} - \dot{\theta}_1) + k_{\mathrm{t}1}(\theta_\mathrm{d} - \theta_1) = T_1, \\
&m_{\mathrm{b}1}\ddot{x}_{\mathrm{b}1} + c_{\mathrm{s}x1}(\dot{x}_{\mathrm{b}1} - \dot{x}_1) + k_{\mathrm{s}x1}(x_{\mathrm{b}1} - x_1) + c_{\mathrm{b}1}\dot{x}_{\mathrm{b}1} \\
&\quad = F_{\mathrm{b}x1}, \\
&m_{\mathrm{b}1}\ddot{y}_{\mathrm{b}1} + c_{\mathrm{s}y1}(\dot{y}_{\mathrm{b}1} - \dot{y}_1) + k_{\mathrm{s}y1}(y_{\mathrm{b}1} - y_1) + c_{\mathrm{b}1}\dot{y}_{\mathrm{b}1} \\
&\quad = F_{\mathrm{b}y1} - m_{\mathrm{b}1}g, \\
&m_{\mathrm{b}1}\ddot{z}_{\mathrm{b}1} + c_{\mathrm{s}z1}(\dot{z}_{\mathrm{b}1} - \dot{z}_1) + k_{\mathrm{s}z1}(z_{\mathrm{b}1} - z_1) + c_{\mathrm{b}1}\dot{z}_{\mathrm{b}1} \\
&\quad = F_{\mathrm{b}z1}.
\end{aligned} \tag{22}
$$

The vibration differential equations of helical gear on driving shaft

$$
\begin{aligned}
&m_1\ddot{x}_1 + c_{\mathrm{s}x1}(\dot{x}_1 - \dot{x}_{\mathrm{b}1}) + c_{\mathrm{s}x2}(\dot{x}_1 - \dot{x}_{\mathrm{b}2}) \\
&\quad + k_{\mathrm{s}x1}(x_1 - x_{\mathrm{b}1}) + k_{\mathrm{s}x2}(x_1 - x_{\mathrm{b}2}) \\
&\quad = -F_x + m_1\rho_1\ddot{\theta}_1 \sin\phi_1 + m_1\rho_1(\omega_1 + \dot{\theta}_1)^2 \cos\phi_1, \\
&m_1\ddot{y}_1 + c_{\mathrm{s}y1}(\dot{y}_1 - \dot{y}_{\mathrm{b}1}) + c_{\mathrm{s}y2}(\dot{y}_1 - \dot{y}_{\mathrm{b}2}) \\
&\quad + k_{\mathrm{s}y1}(y_1 - y_{\mathrm{b}1}) + k_{\mathrm{s}y2}(y_1 - y_{\mathrm{b}2}) = -m_1 g - F_y \\
&\quad - m_1\rho_1\ddot{\theta}_1 \cos\phi_1 + m_1\rho_1(\omega_1 + \dot{\theta}_1)^2 \sin\phi_1, \\
&m_1\ddot{z}_1 + c_{\mathrm{s}z1}(\dot{z}_1 - \dot{z}_{\mathrm{b}1}) + c_{\mathrm{s}z2}(\dot{z}_1 - \dot{z}_{\mathrm{b}2}) \\
&\quad + k_{\mathrm{s}z1}(z_1 - z_{\mathrm{b}1}) + k_{\mathrm{s}z2}(z_1 - z_{\mathrm{b}2}) \\
&\quad = -F_z, \\
&(J_1 + m_1\rho_1^2)\ddot{\theta}_1 + c_{\mathrm{t}1}(\dot{\theta}_1 - \dot{\theta}_\mathrm{d}) + k_{\mathrm{t}1}(\theta_1 - \theta_\mathrm{d}) \\
&\quad = m_1\rho_1\ddot{x}_1 \sin\phi_1 - m_1\rho_1\ddot{y}_1 \cos\phi_1 - Fr_{\mathrm{b}1}.
\end{aligned} \tag{23}
$$

The vibration differential equations on the right bearing of driving shaft and left bearing of driven shaft

$$
\begin{aligned}
&m_{\mathrm{b}2}\ddot{x}_{\mathrm{b}2} + c_{\mathrm{s}x2}(\dot{x}_{\mathrm{b}2} - \dot{x}_1) + k_{\mathrm{s}x2}(x_{\mathrm{b}2} - x_1) + c_{\mathrm{b}2}\dot{x}_{\mathrm{b}2} \\
&\quad = F_{\mathrm{b}x2}, \\
&m_{\mathrm{b}2}\ddot{y}_{\mathrm{b}2} + c_{\mathrm{s}y2}(\dot{y}_{\mathrm{b}2} - \dot{y}_1) + k_{\mathrm{s}y2}(y_{\mathrm{b}2} - y_1) + c_{\mathrm{b}2}\dot{y}_{\mathrm{b}2} \\
&\quad = F_{\mathrm{b}y2} - m_{\mathrm{b}2}g, \\
&m_{\mathrm{b}2}\ddot{z}_{\mathrm{b}2} + c_{\mathrm{s}z2}(\dot{z}_{\mathrm{b}2} - \dot{z}_1) + k_{\mathrm{s}z2}(z_{\mathrm{b}2} - z_1) + c_{\mathrm{b}2}\dot{z}_{\mathrm{b}2} \\
&\quad = F_{\mathrm{b}z2}, \\
&m_{\mathrm{b}3}\ddot{x}_{\mathrm{b}3} + c_{\mathrm{s}x3}(\dot{x}_{\mathrm{b}3} - \dot{x}_2) + k_{s3}(x_{\mathrm{b}3} - x_2) + c_{\mathrm{b}3}\dot{x}_{\mathrm{b}3} \\
&\quad = F_{\mathrm{b}x3}, \\
&m_{\mathrm{b}3}\ddot{y}_{\mathrm{b}3} + c_{\mathrm{s}y3}(\dot{y}_{\mathrm{b}3} - \dot{y}_2) + k_{\mathrm{s}y3}(y_{\mathrm{b}3} - y_2) + c_{\mathrm{b}3}\dot{y}_{\mathrm{b}3} \\
&\quad = F_{\mathrm{b}y3} - m_{\mathrm{b}3}g, \\
&m_{\mathrm{b}3}\ddot{z}_{\mathrm{b}3} + c_{\mathrm{s}z3}(\dot{z}_{\mathrm{b}3} - \dot{z}_2) + k_{\mathrm{s}z3}(z_{\mathrm{b}3} - z_2) + c_{\mathrm{b}3}\dot{z}_{\mathrm{b}3} \\
&\quad = F_{\mathrm{b}z3}.
\end{aligned} \tag{24}
$$

The vibration differential equations of helical gear on driven shaft

$$
\begin{aligned}
&m_2\ddot{x}_2 + c_{\mathrm{s}x3}(\dot{x}_2 - \dot{x}_{\mathrm{b}3}) + k_{\mathrm{s}x3}(x_2 - x_{\mathrm{b}3}) \\
&\quad + c_{\mathrm{s}x4}(\dot{x}_2 - \dot{x}_{\mathrm{b}4}) + k_{\mathrm{s}x4}(x_2 - x_{\mathrm{b}4}) \\
&\quad = F_x + m_2\rho_2\ddot{\theta}_2 \sin\phi_2 + m_2\rho_2(\omega_2 + \dot{\theta}_2)^2 \cos\phi_2, \\
&m_2\ddot{y}_2 + c_{\mathrm{s}y3}(\dot{y}_2 - y_{\mathrm{b}3}) + k_{\mathrm{s}y3}(y_2 - y_{\mathrm{b}3}) \\
&\quad + c_{\mathrm{s}y4}(\dot{y}_2 - \dot{y}_{\mathrm{b}4}) + k_{\mathrm{s}y4}(y_2 - y_{\mathrm{b}4}) = -m_2 g + F_y \\
&\quad + m_2\rho_2\ddot{\theta}_2 \cos\phi_2 - m_2\rho_2(\omega_2 + \dot{\theta}_2)^2 \sin\phi_2, \\
&m_2\ddot{z}_2 + c_{\mathrm{s}z3}(\dot{z}_2 - \dot{z}_{\mathrm{b}3}) + k_{\mathrm{s}z3}(z_2 - z_{\mathrm{b}3}) \\
&\quad + c_{\mathrm{s}z4}(\dot{z}_2 - \dot{z}_{\mathrm{b}4}) + k_{\mathrm{s}z4}(z_2 - z_{\mathrm{b}4}) = F_z, \\
&(J_2 + m_2\rho_2^2)\ddot{\theta}_2 + c_{\mathrm{t}2}(\dot{\theta}_2 - \dot{\theta}_l) + k_{\mathrm{t}2}(\theta_2 - \theta_l) \\
&\quad = m_2\rho_2\ddot{x}_2 \sin\phi_2 + m_2\rho_2\ddot{y}_2 \cos\phi_2 + Fr_{\mathrm{b}2}.
\end{aligned} \tag{25}
$$

The vibration differential equations at output terminal and right bearing of driven shaft

$$
\begin{aligned}
&m_{b4}\ddot{x}_{b4} + c_{sx4}(\dot{x}_{b4} - \dot{x}_2) + k_{sx4}(x_{b4} - x_2) + c_{b4}\dot{x}_{b4} \\
&\quad = F_{bx4}, \\
&m_{b4}\ddot{y}_{b4} + c_{sy4}(\dot{y}_{b4} - \dot{y}_2) + k_{sy4}(y_{b4} - y_2) + c_{b4}\dot{y}_{b4} \\
&\quad = F_{by4} - m_{b4}g, \\
&m_{b4}\ddot{z}_{b4} + c_{sz4}(\dot{z}_{b4} - \dot{z}_2) + k_{sz4}(z_{b4} - z_2) + c_{b4}\dot{z}_{b4} \\
&\quad = F_{bz4}, \\
&J_l\ddot{\theta}_l + c_{t2}(\dot{\theta}_l - \dot{\theta}_2) + k_{t2}(\theta_l - \theta_2) = -T_l,
\end{aligned}
\tag{26}
$$

where k_{sxi}, k_{syi}, and k_{szi} (i = 1, 2, 3, 4) are the bending stiffness of the driving and driven shafts; k_{t1} and k_{t2} represent the torsional stiffness of the driving and driven shafts; c_{sxi}, c_{syi}, and c_{szi} (i = 1, 2, 3, 4) indicate the bending damping of driving and driven shafts; c_{t1} and c_{t2} are the torsional damping of driving and driven shafts; c_{bi} (i = 1, 2, 3, 4) is the bearing damping, F_{xi}, F_{yi}, and F_{zi} (i = 1, 2, 3, 4) indicate the non-linear bearing forces in the x, y, and z directions.

From Eqs. (22) – (26) it can be seen that it is the second-order nonlinear differential equations with 22 degrees of freedom for the helical gears meshing, support bearing and the coupled lateral-torsional-axial vibration.

3 The dynamic response of the HGRBS

From the previous conclusions and analysis, it can be seen that the HGRBS is a complicated system with strong nonlinearity, time variance, the support bearing and complicated working environment. Therefore, it is necessary to give a detailed analysis of the HGRBS. The dynamic behaviors of system are investigated by Runge–Kutta numerical simulation method. In this paper, the model of helical gear-shaft-bearing system is the partial of the MW wind turbine gearbox transmission system, so the geometric parameters of the transmission system are obtained though the actual structure of the 1.5–2 MW wind turbine gearbox transmission system and the dynamical parameters are obtained by material mechanics knowledge and the calculation method of relevant references [22, 23]. On this basis, the parameters are given in Table 1.

By applying the coupled vibration model of the HGRBS, the vibration analysis and calculations are carried out. In this paper, considering the complex nonlinear characteristics (the meshing stiffness, input and output torques, meshing error, nonlinear characteristics of the support bearing and gravity effects and so on), the analytical model of helical gear-rotor-bearing system is investigated using the Runge–Kutta numerical simulation method, which can be used to systematically study the vibration characteristics of HGRBS with changing rotational speed, eccentricity and bearing clearance. This method, together with the elastic mechanics theory, is applied to constitute a lumped-parameter HGRBS model. A coupled dynamic mechanical analysis is performed, which considers all the components of influence factors.

Table 1 Structure and dynamic parameters of helical gear-rotor-bearing transmission system

Gear parameters		
Number of teeth	z_1	100
	z_2	25
Mass/kg	m_1	667.89
	m_2	141.038
Inertia/(kg·m^{-2})	J_1	44.35
	J_2	0.207
Eccentricity/m	ρ_1	5.0×10^{-5}
	ρ_2	5.0×10^{-5}
Mesh stiffness/(N·m^{-1})	k_m	6.0×10^{8}
Meshing damping ratio	ξ_m	0.1
Gravity acceleration	g	9.8
Pressure angle/(°)	α_t	23.2
Pitch circle helix angle/(°)	β	15
Base helix angle/(°)	β_b	13.8
Position angle/(°)	α_1	120
Shaft parameters		
Torsional stiffness	k_{t1}	8×10^{8}
	k_{t2}	1.5×10^{8}
Torsional damping ratio	ξ_t	0.07
Bending stiffness	k_{s1}, k_{s2}	6.513×10^{8}
	k_{s3}, k_{s4}	0.157×10^{8}
Bending damping ratio	ξ_s	0.07
Input/out parameters		
Input/out rotational inertia	J_d	20
	J_1	5
Input/out speed/(r·min^{-1})	n_1	500
	n_2	2 000
Transmission error		
Mean/m	e_m	2×10^{-5}
Amplitude/m	e_r	3×10^{-5}
rotation rate/(r·min^{-1})	ω_e	2 000
Bearing parameters		
Lumped mass/kg	m_{b1}, m_{b2}	115.2
	m_{b3}, m_{b4}	73.2
Bearing stiffness/(N·m^{-1})	k_{bx1}, k_{bx2}	6×10^{8}
	k_{by1}, k_{by2}	9×10^{8}
	k_{bz1}, k_{bz2}	4.8×10^{8}
Bearing stiffness/(N·m^{-1})	k_{bx3}, k_{bx4}	2×10^{8}
	k_{by3}, k_{by4}	3×10^{8}
	k_{bz3}, k_{bz4}	1.6×10^{8}
Bearing damping ratio	ξ_b	0.01
Bearing contact stiffness	k_{b1}	13.34×10^{7}
	k_{b2}	10.34×10^{7}
Bearing outer/inner radius/m	R_1	0.25
	r_1	0.2
Bearing outer/inner radius/m	R_2	0.125
	r_2	0.1

Figures 5 and 6 are respectively the time-domain waveform and the frequency domain response of the driving and driven helical gears and the corresponding dynamic response of the left bearing in the x, y, and z directions (local frequency domain response is shown in some figure) for rotational speed $n_1 = 500$ r/min. x_1, y_1, and z_1 represent the driving helical gear linear vibration displacements in three directions. x_{b1}, y_{b1}, and z_{b1} are the corresponding left bearing linear vibration displacements in the x, y, and z directions. x_2, y_2, z_2; x_{b2}, y_{b2}, and z_{b2} indicate the linear vibration displacements of the corresponding driven gear and bearing. It can be seen from Fig. 5 that driving gear and bearing show slightly different vibration response in the x, y, and z directions. By comparing the waveforms between driving gear (Figs. 5a$_1$–5c$_1$) and bearing (Figs. 5d$_1$–5f$_1$), it can be seen that the waveform change trend has a little difference, but the vibration amplitudes have significantly difference. It can be seen from the frequency spectrograms between driving gear (Figs. 5a$_2$–5c$_2$) and bearing (Figs. 5d$_2$–5f$_2$) that the frequency components also have significantly difference. The vibration amplitude in the y direction is higher than that in the x and z directions. In addition, the main frequency of vibration in the y direction is significantly higher than those in the x and z directions, in which the high-order harmonic components appear. From the frequency domain response of the driving gear and bearing, it can be seen that the driving

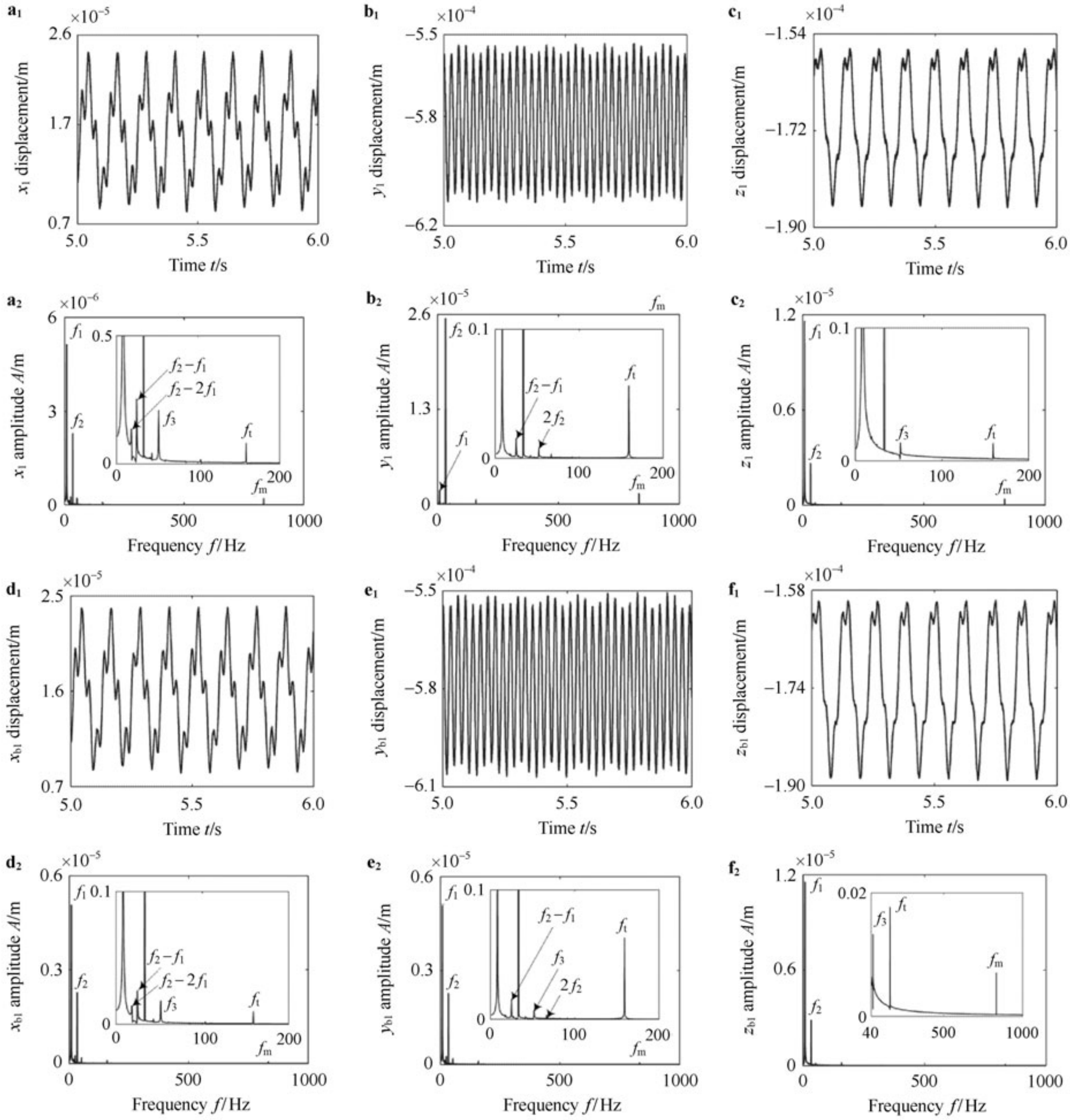

Fig. 5 Lateral and axial vibration waveform and frequency of the driving gear and bearing

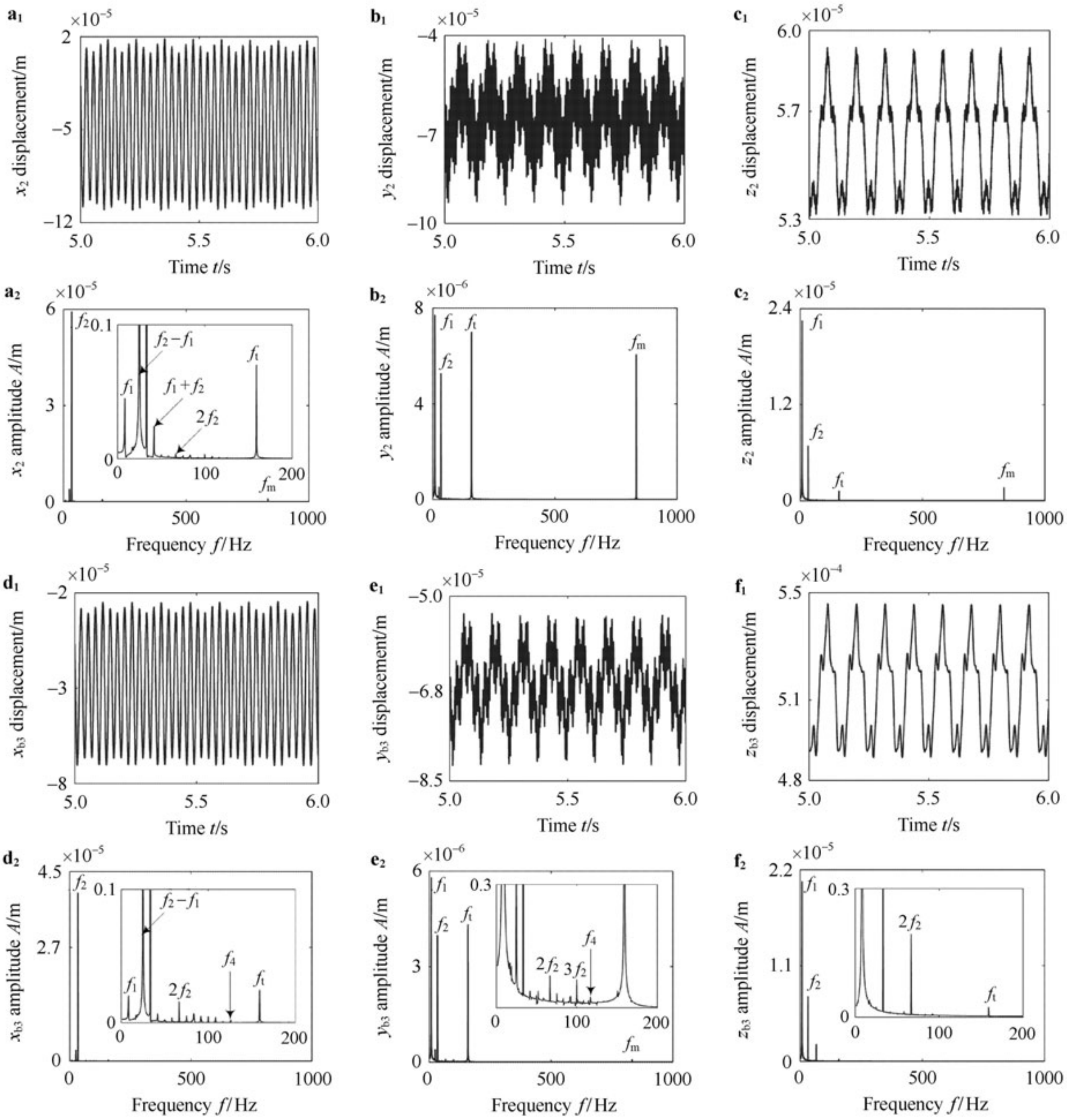

Fig. 6 Lateral and axial vibration waveform and frequency of the driven gear and bearing

shaft rotational frequency f_1 ($n_1/60 = 8.3\,\text{Hz}$) is the main frequency in the x and z directions, and the driven rotational frequency f_2 ($n_2/60 = 33.3\,\text{Hz}$) is the main frequency in the y direction. Moreover, the two rotational frequency components (f_1, f_2) appear in all directions. The input/output frequency component f_t ($\omega/(2\pi) = 159\,\text{Hz}$) and the bearing variable stiffness frequency f_3 (52 Hz) appear in the z direction of driving shaft and bearing. However, the frequency features become more complicated in the x and y directions, in which the frequency combination $f_2 - f_1$(25 Hz) and the frequency multiplication $2f_2$ (66.7 Hz) also appear. In addition, a high-frequency component f_m (meshing frequency $n_1 z_1/60 = 833.3\,\text{Hz}$) appears in three directions, but this component is relatively weak. This comparison proves that the frequency components in the z direction are relatively simpler than those in the x and y directions, which shows larger amplitude of low-speed shaft frequency f_1, a smaller amplitude of high-speed shaft frequency f_2 and gear meshing frequency f_m.

The lateral and axial vibration responses of driven gear and bearing are shown in Fig. 6. It can be seen from Fig. 6 that the vibration waveforms in the x, y, and z directions have an obvious difference between the driven shaft and bearing. Compared with the driving shaft, the main frequency component in the x direction is higher. However, the waveform in the y direction is a superposition of several frequencies (which can be confirmed by referring to the spectrum), and the low frequency component in the z direction is the main response. The amplitude in the y direction is obvious higher than those in the x and z directions, which are the same as those of driving shaft. The mesh form of helical gears and coordinate system has a significant influence on the dynamic behavior. In Figs. 6a$_2$–6f$_2$, the rotational frequencies f_1 and f_2, are the main frequency components in the x direction, and the frequencies combination $f_2 - f_1$ (25 Hz), $f_2 + f_1$ (41.7 Hz) and $2f_2$ also weakly appear. The rotational frequencies, the meshing frequency f_m and torsional frequency f_t also appear in the y direction. The frequency components in the z direction are simpler than others. For the driven bearing, the rotational frequency component of driven shaft is obvious, and the f_1, frequency combination $f_2 - f_1$, frequency multiplication $2f_2$ also appear. Besides, the variable stiffness frequency f_4 of the driven bearing and the input/output frequency component f_t have a little difference in the x direction. However, the frequency components in the y direction become more complicated, which includes more obvious rotational frequencies of driving and driven shafts and the input/output frequency component. In addition, the frequency multiplication $2f_2$, $3f_2$, variable stiffness frequency and other frequency combination components also appear.

Figure 7 shows the torsional vibration responses of the driving and driven gears. From the waveforms it can be seen that the torsional vibration of the driving helical gear is positive, and it is negative for the driven helical gear, which is mainly caused by the selection of the meshing direction. Pinion torsional amplitude is bigger because of the different torsional stiffness of shaft. From the frequency domain response it can be seen that the rotational frequencies of two shafts, the input/output frequency and the meshing frequency are shown in Figs. 7a$_2$ and 7b$_2$, in which the meshing frequency of driving shaft is considerably higher than that of the driven shaft, and the frequency components amplitude are much different between driving shaft and driven shaft.

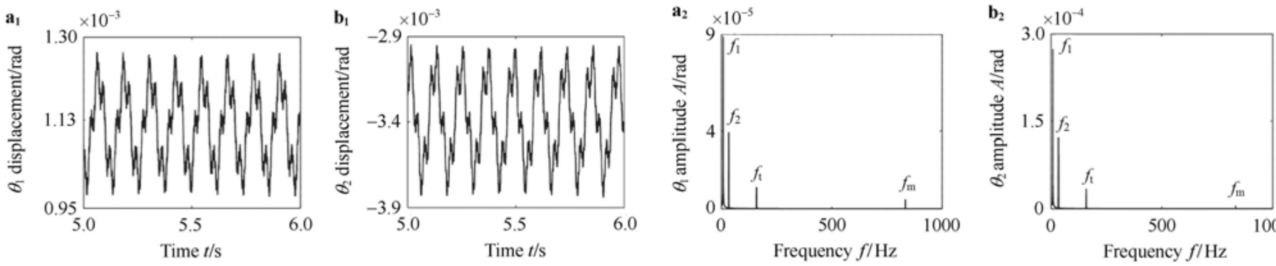

Fig. 7 Torsional vibration waveform and frequency of the driving/driven gears

From the above response analysis of the HGRBS, it can be seen that the lateral, torsional and axial vibration responses and bearings behaviors are obviously different due to the influence of the gear assembly characteristics, gear geometry parameters and the angular contact ball bearings characteristics. Difference appears not only in the rotational frequencies and meshing frequency, but also in the bearing variable stiffness frequency and frequencies combination in all direction, which makes the vibration waveforms more complicated. Due to the influence of the coupled lateral-torsional-axial vibration, the lateral harmonic frequencies (rotational frequencies and meshing frequency) appear in the rotational directions, but the bearing variable stiffness frequency does not appear. In order to correctly analyze and investigate nonlinear characteristics of the systems, it is necessary to systematically study the influences of rotational speed, gear eccentricity and bearing clearance on the coupled lateral, torsional and axial vibration, which are discussed in the following sections.

3.1 Dynamics response of HGRBS with changing rotational speed

Figures 8–10 are respectively the time-domain waveforms and the frequency domain responses at rotational speed $n_1 =$ 700 r/min. Comparing Figs. 5, 6 with Figs. 8, 9, the vibration characteristics of the driving and driven gears have a lot of changes in the x, y, and z directions when the rotational speed changes. Due to the changes of gears and bearings are basically identical, only the variation curves of gear are given. As can be seen from Fig. 8, the harmonic components have obvious difference in vibration waveforms. Namely, not only the higher-order harmonic components show some decrease, but also the vibration amplitudes have grown to some extent in the x direction. The vibration amplitude in the y direction is higher than those in the x and z directions (it is in accordance with the present analysis), and the waveform becomes more complicated. Meanwhile the waveform has little differences in the z direction.

In the figures of frequency domain response, the frequency combination and frequency multiplication of the driving and driven shafts obviously appear in the x and y directions, in which the rotational frequency f_1 is the main frequency. The waveform has no obvious change in the y direction, where the rotational frequency f_2 is the main frequency, and the frequency combination $(f_2 - f_1)$ has lowered to some degree. In addition, the input/output frequency and meshing frequency components are contained in all directions.

Figure 9 shows dynamic response of the driven helical gear. Comparing Fig. 9 with Fig. 6, the vibration amplitudes of driven gear have obvious increase in the x and y directions, which are similar to those of driving gear. However, the vibration features have no obvious change in the z direction. In the frequency domain, it can be seen that the driving shaft rotational frequency f_1 is the main frequency in the x direction, and the $2f_1$ component becomes more obvious. However, the rotational frequency f_1 is also the main frequency in the y and z directions. With the change of rotational speed, the frequency features will become more complicated in the y direction, in which the frequency multiplication ($2f_2$) and the bearing variable stiffness frequency f_3 of driving bearing are shown obviously but the driven bearing variable stiffness frequency f_4 can not be seen clearly, at the same time, the meshing frequency f_m becomes lower. The $2f_2$ also appears in the z direction, but the other frequency components have little change. The frequency features of the driven bearing become more complicated in the x and y directions, where frequency multiplication and frequency combination present more obvious differences. However, we find significant change in the driven bearing variable stiffness frequency f_4 in the x direction, and the frequency f_4 becomes weak in the y direction. f_1, f_2, f_t, and f_m are also the main frequency components in the z direction, and the frequency amplitudes have little increase.

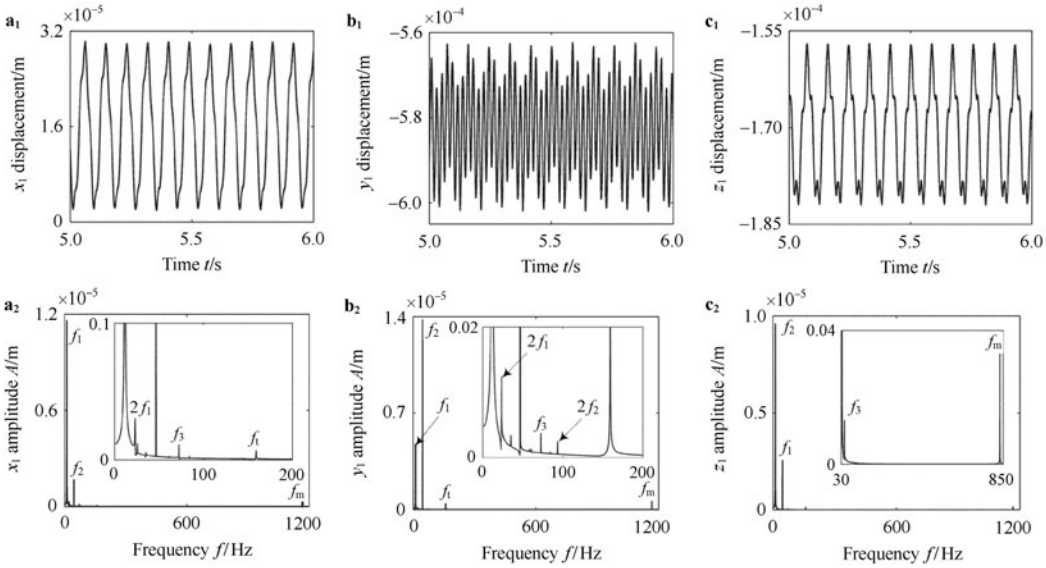

Fig. 8 Lateral and axial vibration waveform and frequency of the driving gear and bearing

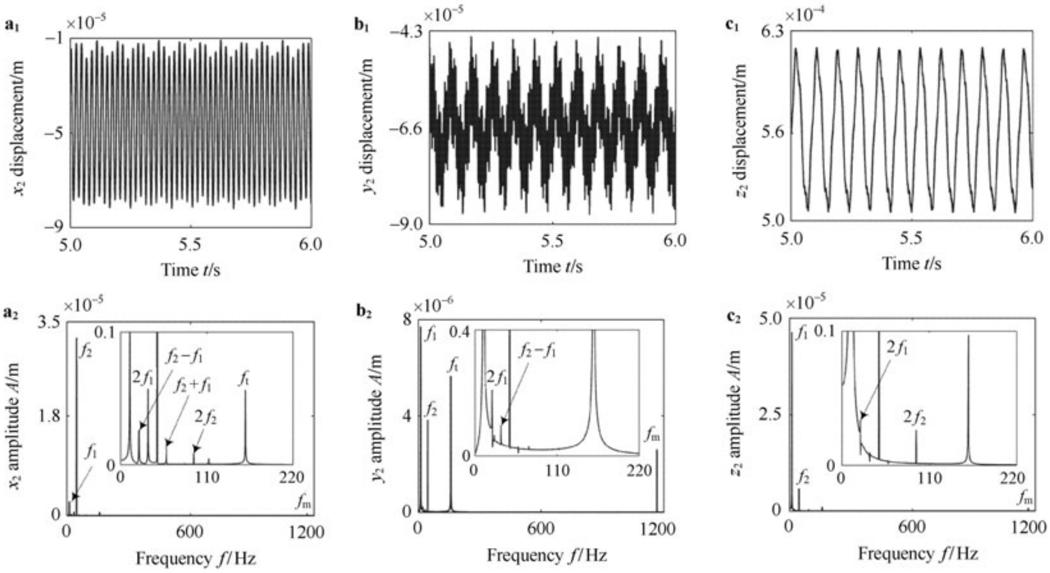

Fig. 9 Lateral and axial vibration waveform and frequency of the driven gear and bearing

The torsional vibration responses of the driving and driven helical gears are shown in Fig. 10 for the driving rotational speed of 700 r/min. Comparing Fig. 7 with Fig. 10, the positive and negative torsional vibration responses have no difference with the rotational speed fluctuation of driving shaft, and the vibration amplitudes have little increase. In the frequency domain, it can be seen that the rotational frequencies f_1, f_2, the input/output frequency f_t and the meshing frequency f_m are also the main frequencies. In addition, the rotational frequency of driving shaft is higher than the others and the difference between driving and driven rotational frequency becomes slight.

The above part makes a detailed analysis and description about the vibration response characteristics with $n_1 = 500$ r/min and $n_1 = 700$ r/min. In order to accurately analyze the dynamics of the HGRBS with rotational speed, three-dimensional plots of the system are shown in Figs. 11 and 12 for different rotational speed. With increasing rotational speed, the meshing frequency f_m in the x, y, and z directions decrease first, and then increase (the meshing frequency has a general trend of decreasing with the change of the rotational speed in the three-dimensional plots of frequency spectrum), and the frequency amplitude reaches a minimum value when the rotational speed of driving gear is 650 r/min. The rotational frequency f_1 is the main frequency in the x direction, which decreases first, and then increases and reaches the minimum when the rotational speed of driving gear is 500 r/min. In addition, the bearing variable stiffness frequency has no obvious change. The rotational frequency f_2 is also the main frequency in the y direction,

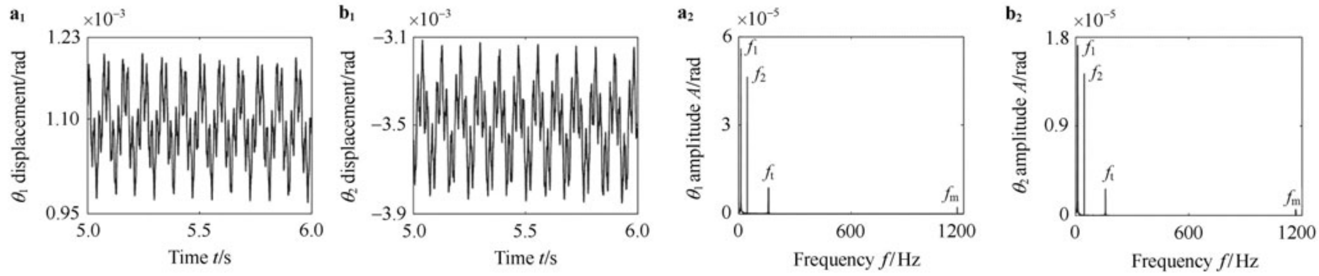

Fig. 10 Torsional vibration waveform and frequency of the driving/driven gears

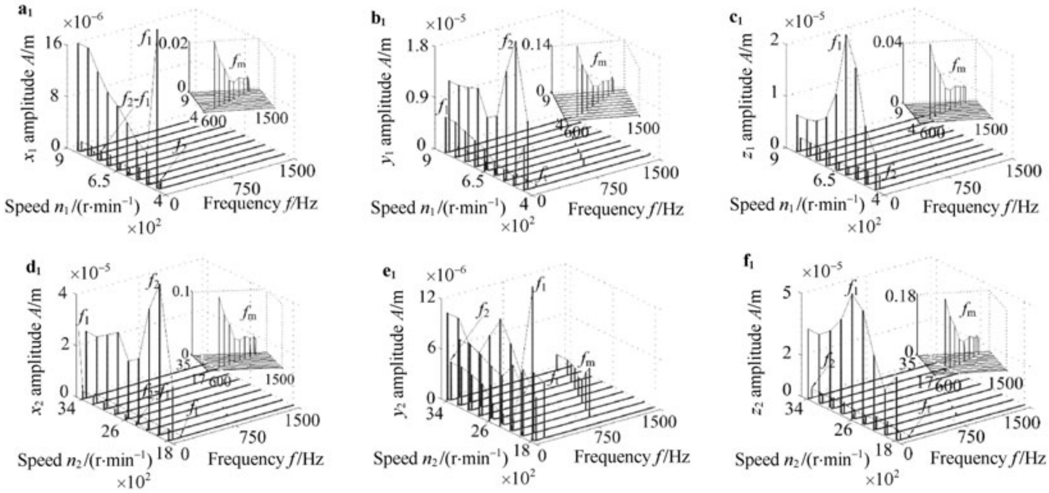

Fig. 11 Lateral vibration 3-D spectrum diagram of the master/slave gears and bearings

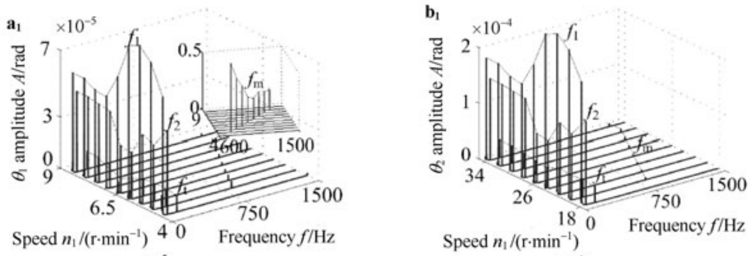

Fig. 12 Torsional vibration 3-D spectrum diagram of the gears

the frequency f_2 increases first, and then decreases with the change of the rotational speed. The frequency amplitude reaches a peak value when the driving rotational speed $n_1 = 500$ r/min, and the frequency f_1 is increasing gradually. The rotational frequency f_2 is the main frequency in the z direction. With increasing rotational speed, the frequency f_2 is increasing. The frequency amplitude reaches the maximum when the rotational speed of driving shaft $n_1 = 650$ r/min. For the driven shaft, the meshing frequency component f_m has a similar changing trend in the x, y, and z directions. The rotational frequency f_2 is the main frequency in the x direction. With increasing rotational speed, the frequency f_2 increases first, and then decreases, and the frequency amplitude reaches a peak value when the driven rotational speed $n_2 = 2\,000$ r/min. The frequency combination components $(f_2 - f_1, \cdots)$ have no obvious fluctuation, and the bearing variable stiffness frequency f_4 does not show any obvious change. In the y direction, the frequencies have obvious fluctuation with changing rotational speed, and the frequency f_1 is the main frequency. In the z direction, the frequency f_1 reaches the maximum when the driven rotational speed $n_2 = 2\,600$ r/min, while other frequencies have no significant change. Figure 12 shows torsional three-dimensional plots of frequency spectrum of the gears. It can be seen that the rotational frequencies, input/output frequency and meshing frequency appear obviously, and the rotational frequency f_1 increases first, and then decreases, and the amplitude of frequency f_1 has a peak value when the rotational speed of driven gear is $2\,400$ r/min. What is more, the rotational frequency f_2 decreases and then increases, which reaches the minimum when the rotational speed of driving shaft is 600 r/min. The meshing frequency of the driven shaft decreases first, and then increases, but it is obviously different from that of the driving shaft. The amplitude of frequency f_2 is much larger than that of the driving shaft frequency. Through comparing Fig. 11 with Fig. 12, it can be seen that the rotational frequency components are the main characteristics of two shafts in the x direction. The other frequency components are the main factors in the y direction, but its own frequency is not gradually weakened. The rotational frequency component of driving shaft is the main frequency in the z direction, which is the same as the result of previous analysis. Besides, with the increase of speed, the meshing frequency f_m gradually decreases, and other frequencies present different trends.

3.2 Dynamics response of HGRBS with changing eccentricity

In this section, the eccentricity of driving and driven gears enhances from $\rho_1 = \rho_2 = 50\,\mu$m to $\rho_1 = \rho_2 = 100\,\mu$m. Figures 13–15 are the vibration responses of the HGRBS. Through comparing Figs. 5 and 6 with Figs. 13 and 14, the vibration characteristics and frequency components of gears have obvious differences in the x, y, and z directions when the driving and driven gears eccentricity enhances, especially the vibration amplitude of driven gear increases significantly, but the fluctuation trend is almost unchanged. For the driving gear, the vibration amplitude in the y direction is obviously higher than those in the x and z directions. It also can be found from the spectrogram (Fig. 13) that the rotational frequency f_1 is still the main frequency in the x direction. In addition, the frequency combination components $(f_2 - f_1, f_2 + f_1, \cdots)$, frequency multiplication $2f_1$ and the driving bearing variable stiffness frequency f_3 also increases significantly, but the torsional frequency f_t reduces. The frequency amplitudes are doubled in the y direction and the frequency components become more complicated (some components need to enlarge). Besides, a large number of frequency components also appear (the rotational frequencies f_1, f_2, the frequency multiplication $2f_1$, $2f_2$, $3f_2$, the frequency combination components $f_2 - f_1$, $f_2 + f_1$, the driving bearing variable stiffness frequency f_3 and the input/output frequency component f_t). In the z direction of driven shaft gear, in addition to the original frequency components (f_1, f_2, f_3, f_t), some new frequency components $(f_2 - f_1, 2f_2, 3f_2, \cdots)$ are presented with the change of eccentricity.

Comparing Fig. 13 with Fig. 6, it can be found that the vibration amplitudes become higher in the x, y, and z directions when the gear eccentricities increase, but the harmonic components of waveform have no obvious change. This comparison proves that the frequency combination and the frequency multiplication components become more obvious and the vibration amplitudes are doubled. The frequency components in the y direction become more complicated. The main frequencies are composed of rotational frequencies and the input/output frequency. In addition, the frequency multiplication $(2f_2, 3f_2, \cdots)$ and the frequency combination components $(f_2 - f_1, f_2 + f_1, \cdots)$ are more prominent. With the increase of gear eccentricity, the rotational frequency f_1 becomes the main frequency in the z direction and frequency multiplication components also appears. According to the above analysis, it can be found that the vibration characteristics of the driven shaft are similar to that of the driving shaft, which may be ascribed to the flexibility of shafts.

Comparing Fig. 15 with Fig. 7, it can be found that the torsional vibration amplitudes of driving and driven shafts increase obviously, but the waveforms have no obvious fluctuation. Besides, this comparison of rotational frequencies proves that the frequency components have no obvious change. However, the amplitudes of the rotational frequencies, the input/output frequency and the meshing frequency components are increased, even doubled. The frequency components of driven are relatively high in the rotational spectrum diagram, which is related to the flexibility of driven shaft. Therefore, it can be seen that the eccentricity has obvious effect on the amplitudes of the gear in the rotational direction, which is a fundamental proportional relation and will be analyzed in detail in the following.

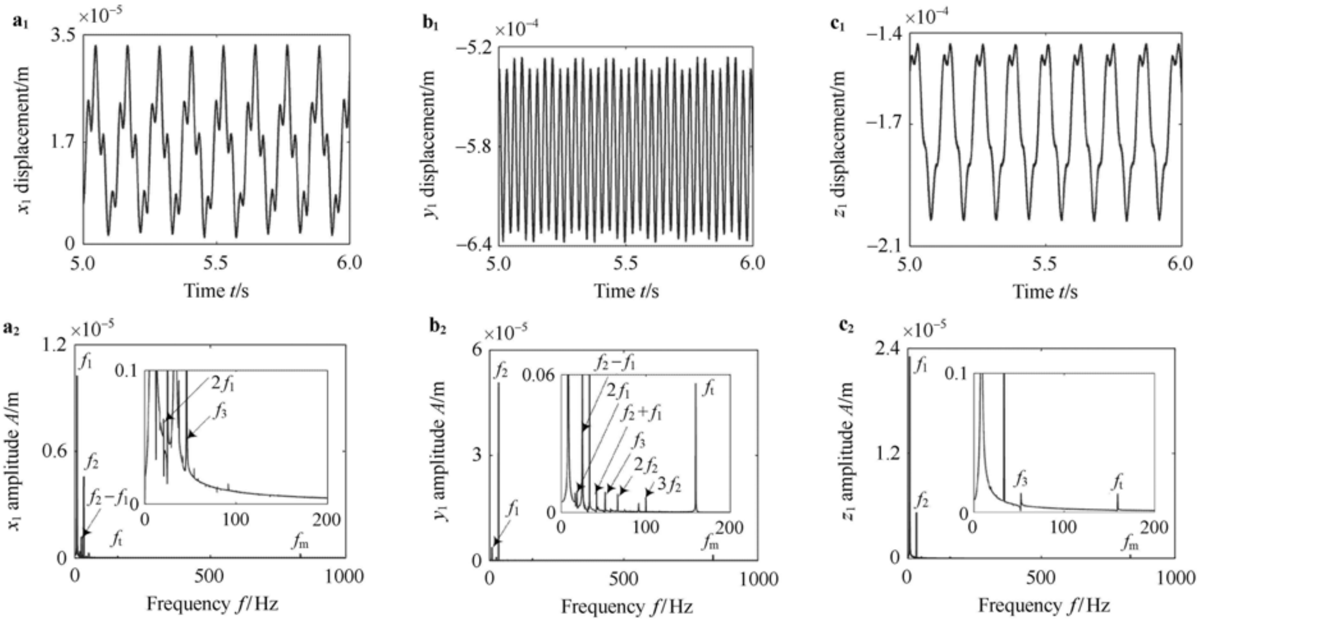

Fig. 13 Lateral and axial vibration waveform and frequency of the driving gear and bearing

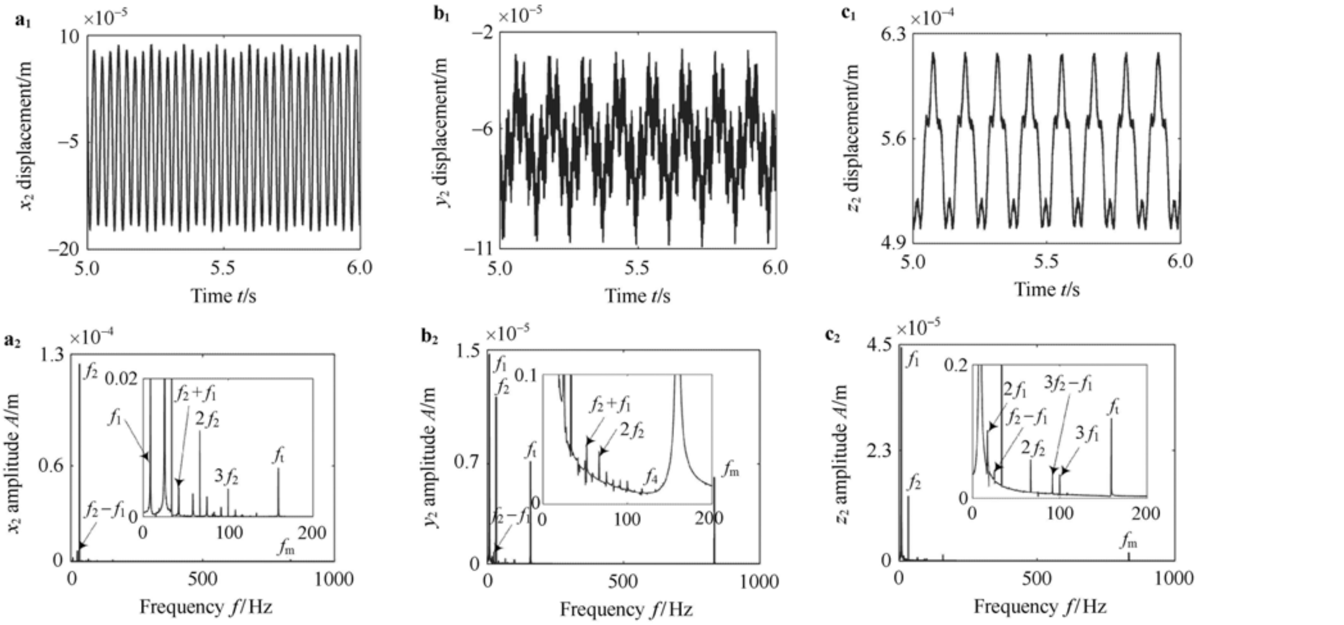

Fig. 14 Lateral and axial vibration waveform and frequency of the driven gear and bearing

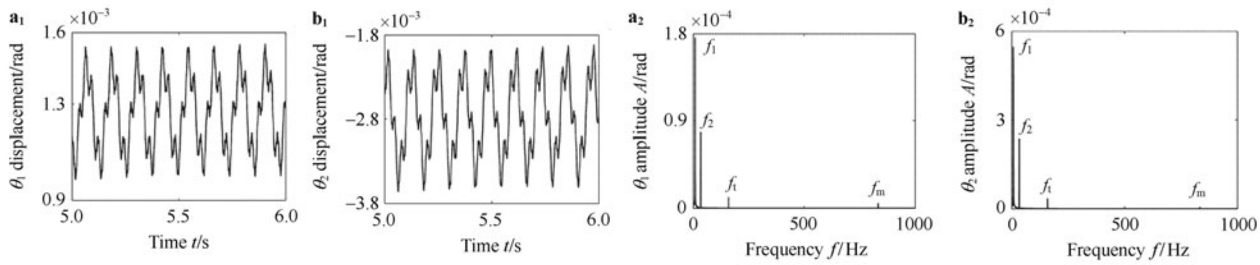

Fig. 15 Torsional vibration waveform and frequency of the driving/driven gears

In above sections, the response characteristics are analyzed for $\rho_1 = \rho_2 = 50\,\mu\mathrm{m}$ and $\rho_1 = \rho_2 = 100\,\mu\mathrm{m}$. In order to study the effect of the eccentricity, three-dimensional plots of frequency spectrum of the gears in all directions are shown in Figs. 16 and 17. It can be seen from Fig. 16 that the frequency components of driving and driven shafts have obvious differences, which are due to the change of eccentricity, but not monotonously increasing with the increase of eccentricity. For the driving gear, the rotational frequencies attain the minimum when the eccentricities reach $\rho_1 = \rho_2 = 60\,\mu\mathrm{m}$ in the x direction, but the bearing variable stiffness frequency component f_3 has no obvious change. The rotational frequency amplitudes of driving and driven shafts increase gradually with the increase of eccentricity in the y direction, and the meshing frequency components f_m reflects the growth of the fluctuation. The rotational amplitude spectrogram of driving shaft also has obvious fluctuation in the z direction, but f_3 is the main frequency and other frequencies have no obvious change. For the driven gear, the rotational frequency f_2 becomes the main frequency in the x direction, which is due to the high rotational speed of driven shaft. Besides, the rotational frequency amplitude, which present a state of fluctuation, increase with the change of the eccentricity. The meshing frequency component f_m is very obvious in the y direction and the frequency multiplication and random spectrum components are more and more obvious, moreover, the rotational frequency f_1 also becomes more obvious. For the bearing, the frequency amplitudes are similar to those of the driving and driven gears when the eccentricity changes (It will not be reiterated here.). The rotational frequencies (f_1, f_2), the meshing frequency f_m, and the input/output frequency components are the main frequencies in the rational direction. In addition, the frequency amplitudes increase gradually and the driven amplitude is higher than that of the driving shaft. Based on the above analysis, with the change of eccentricity, the frequency components at all positions are increasing, but they are not monotonously increasing, and the variational pattern of frequency is basically identical. The meshing frequency and the input/output frequency components have a little fluctuation and no significant effects were found with change of eccentricity.

3.3 Dynamic response of HGRBS with changing bearing clearance

This section will analyze the influence of the bearing clearance. The vibration characteristics caused by change of bearing clearance are similar to the forgoing ones, because of the limited space, this paper does not discuss the time domain response, and Figs. 18 and 19 are three-dimensional plots of

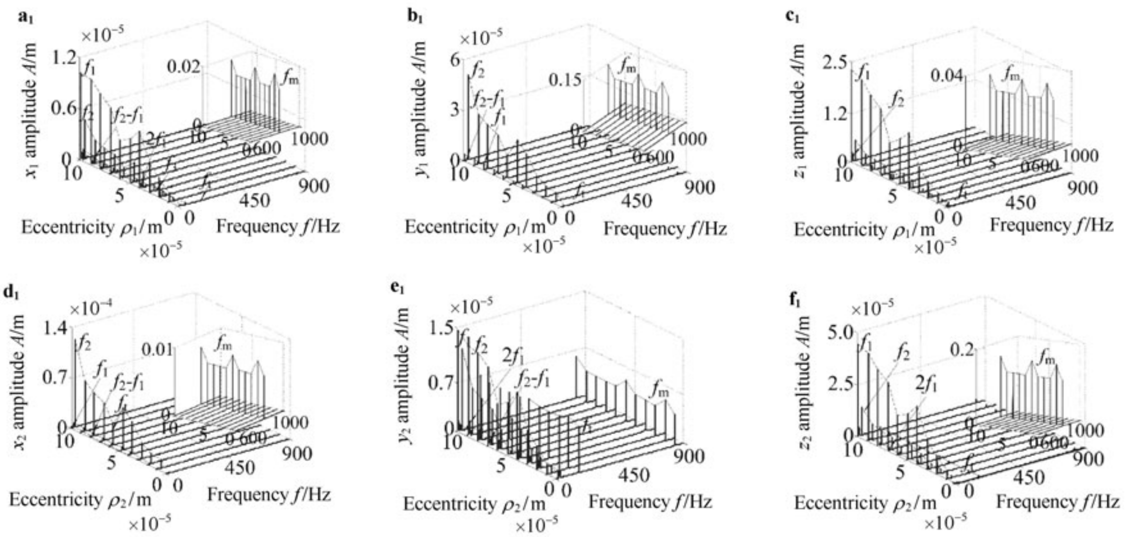

Fig. 16 Lateral vibration 3-D spectrum diagram of the master/slave gears and bearings

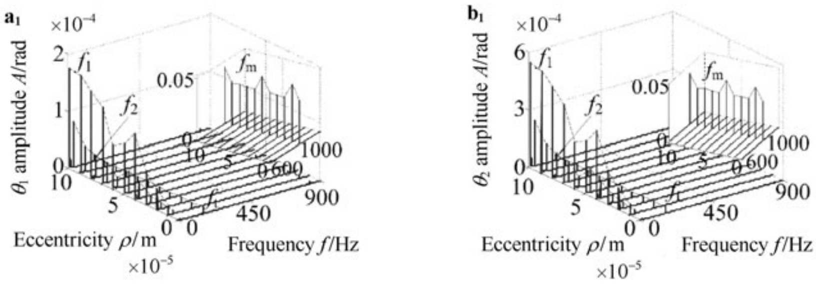

Fig. 17 Torsional vibration 3-D spectrum diagram of the gears

the frequency spectrum at key positions. For the driving gear, it can be found that the amplitude of rotational frequency f_1 increases first, and then decreases with the change of the bearing clearance, but the behavior has no obvious change in the x direction. Moreover, $2f_1$ grows continually. The rotational frequency f_2 and the meshing frequency f_m are obvious in the y direction, but the variation trend of amplitude has no obvious difference. The bearing variable stiffness frequency f_3 also appears. In the z direction, the rotational frequencies f_1, f_2 are the main components, and the bearing variable stiffness frequency, the frequency combination and the rotational frequency multiplication are relatively lower. Besides, with increasing bearing clearance, the amplitudes of the rotational frequencies increase first, and then decrease, but the meshing frequency remains almost unchanged. The results show that the driving bearing features are similar to the driving rotational frequency. Due to the nonlinear characteristic of bearing, the frequency multiplication and the random frequency become obvious near f_1 (so it will not be reiterated). For the driven shaft, because of the high rotational speed, the driven rotational frequency, the bearing frequency and other components appear obviously. The frequency component is relatively simple in the x direction, in which the rotational frequency f_2 is the main frequency and others are not obvious. The frequency f_2 attains the minimum when the bearing clearance reaches 60 μm. With increasing bearing clearance, the frequency amplitude in the y direction increases first, and then decreases as well. The meshing frequency f_m, the frequency multiplication and frequency combination components are more and more obvious. The driving rotational frequency f_1 is the main frequency and other frequency components become more complicated in the z direction. The torsional three-dimensional plots of frequency spectrum of the gears are shown in Fig. 19. It can be seen that the torsional frequency amplitudes and the stiffness frequency amplitude remain almost unchanged. Based on the results obtained in the previous sections, it can be seen that the bearing clearance has a little effect on the driving gear characteristics in the x and z directions. Moreover, the vibration responses are not sensitive to bearing clearance. Therefore, it needs little attention in related designs.

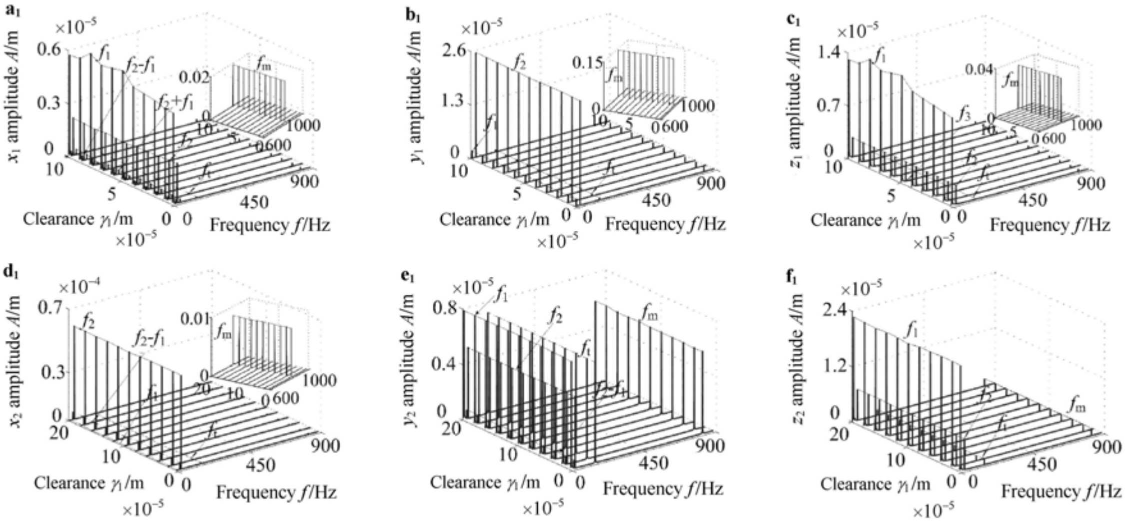

Fig. 18 Lateral vibration 3-D spectrum diagram of the driving/driven gears and bearings

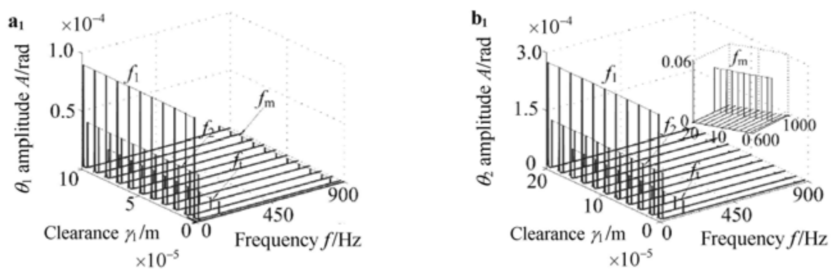

Fig. 19 Torsional vibration 3-D spectrum diagram of the driving/driven gears

4 Conclusion

In this paper, a lumped-parameter mathematical model is used to numerically analyze the nonlinear dynamic characteristics of coupled lateral-torsional-axial vibrations for the helical gear transmission system, and vibration responses of the system was investigated systematically by changing speed, eccentricity and bearing clearance. Based on the results of the parametric study presented in the previous sections, conclusions can be summarized as follows:

(1) Because of the axial force, there is a close coupling relationship between the lateral and the torsional vibrations of the HGRBS. Hence, for the HGRBS, it is necessary to take into account the coupled lateral-torsional-axial vibration.

(2) Due to the influence of coupled lateral, torsional and axial vibrations, an obvious rotational frequency component of driven shaft yields in the driving shaft. At the same time, the rotational frequency of driving shaft appears in the driven shaft. The rotational frequencies and the input/output frequency components are more obvious in the torsional direction, which has different characteristics with the change of the rotational speed. The bearing has its own resonance frequency, and the effect of the variable stiffness frequency of the bearings in system should be avoided in the system design stage.

(3) With the increase of the eccentricity, the rotational amplitude spectrograms are not increasing monotonously in the lateral and torsional directions. Besides, the frequency multiplication and the random frequency become more and more obvious at the bearing position. The bearing clearance has no obvious effect on the vibration response of the system. Therefore, the bearing clearance needs little attention in engineering design.

References

1 Lmi, T.C., Cheng, Y.A.: A theoretical study of the effect of pinion offset on the dynamics of hypoid geared rotor system. Transactions of the ASME, Journal of Mechanical Design **121**, 535–539 (1999)
2 Li, M., Yu, L.: Analysis of the coupled lateral torsional vibration of a rotor-bearing system with a misaligned gear coupling. Journal of Sound and Vibration **243**, 283–300 (2001)
3 Guan, Y.H., Li, M.F., Lim, T.C., et al.: Comparative analysis of actuator concepts for active gear pair vibration control. Journal of Sound and Vibration **169**, 273–294 (2004)
4 Kaharman, A., Singh, R.: Non-linear dynamicas of a spur gear pair. Journal of Sound and Vibration **142**, 49–75 (1990)
5 Kaharman, A., Singh, R.: Non-linear dynamicas of a geared rotor-bearing system with multiple clearances. Journal of Sound and Vibration **144**, 4469–4506 (1991)
6 Al-shyyab, A., Kahraman, A.: Non-linear dynamic analysis o a multi-mesh gear train using multi-term harmonic balance method: Sub-harmonic motions. Journal of Sound and Vibration **279**, 417–456 (2005)
7 Lin, H.H., Oswald, F.B., Townsend, D.P.: Dynamic loading of super gear with linear or parabolic tooth profile modification. Journal of Mechanisms Transmissions and Automation in Design **29**, 1115–1129 (1994)
8 Rao, J.S., Shiau, T.N., Chang, J.R.: Theoretical analysis of lateral response due to torsional excitation of geared rotors. Mechanism and Machine Theory **33**, 761–783 (1998)
9 Wang, L.H., Li, R.F., Lin, T.J., et al.: Analysis for coupled vibration of helical gear transmission system. Machine Design and Research **18**, 30–31 (2002)
10 Mamla, R., Do, G., Zgnven, H.N.: Nonlinear dynamic modeling of gear shaft disk bearing systems using finite elements and describing functions. ASME, Journal of Mechanical Design **263**, 534–541 (2004)
11 Lee, A.S., Ha, J.W., Choi, D.H., et al.: Coupled lateral and torsional vibration characteristics of a speed increasing geared rotor-bearing system. Journal of Sound and Vibration **263**, 725–742 (2003)
12 Jiang, Q.L., Wu, D.Z., Tan, S.G., et al.: Development and application of a model for coupling geared rotors system. Journal of Vibration Engineering **23**, 254–259 (2010)
13 Dou, W., Zhang, N., Liu, Z.S.: The coupled bending and torsional vibrations of the high-speed geared rotor-bearing system. Journal of Vibration Engineering **24**, 385–393 (2011)
14 Che, Y.Q., Xu, J.X., Qian, X.D., et al.: Coupled bending and torsional vibrations of gear rotor system. Journal of Mechanical & Electrical Engineering **29**, 632–635 (2012)
15 Wang, Q., Zhang, Y.D.: Coupled analysis based dynamic response of two-stage helical gear transmission system. Journal of Vibration and Shock **10**, 87–91 (2012)
16 Lee, A., Ha, J.W.: Prediction of maximum unbalance responses of a gear-coupled two-shaft rotor-bearing system. Journal of Sound and Vibration **282**, 07–523 (2005)
17 Chen, Z.G., Shao, Y.M., Lim, T.C.: Non-linear dynamic simulation of gear response under the idling condition. International Journal of Automotive Technology **13**, 541–552 (2012)
18 Wu, M.J., Zuo, A.P.: Simulation of spur gear dynamic and estimation of fault growth. Journal of Sound and Vibration **17**, 608–624 (2008)
19 Walha, L., Fakhfakh, T., Haddar, M.: Nonlinear dynamics of a two-stage gear system with mesh stiffness uctuation, bearing exibility and backlash. Mechanism and Machine Theory **44**, 1058–1069 (2008)
20 Russo, R., Brancati, R., Rocca, E.: Experimental investigations about the influence of oil lubricant between teeth on the gear rattle phenomenon. Journal of Sound and Vibration **3**, 647–661 (2009)
21 Han, B.K., Cho, M.K., Lim, C.H., et al.: Prediction of vibrating forces on meshing gears for a gear rattle using a new multi-body dynamic model. Journal of Automotive Technology **10**, 469–474 (2009)
22 Kubur, M., Kahraman, A., Zini, D.M., et al.: Dynamical analysis of a multi-shaft helical gear transmission by finite elements: model and experiment. ASME Journal of Vibration and Acoustics **126**, 398–406 (2004)
23 Farag, K.O., Kamal, A.F., Samir, E.: Mathematical modeling of gearbox including defects with experimental verification. Journal of Vibration and Control **18**, 1310–1321 (2012)